Applied Catalysis B: Environmental 331 (2023) 122671

Contents lists available at ScienceDirect

Applied Catalysis B: Environmental

journal homepage: www.elsevier.com/locate/apcatb

# Waste PVC upcycling: Transferring unmanageable Cl species into value-added Cl-containing chemicals

Bo Feng, Yaxuan Jing *, Xiaohui Liu, Yong Guo, Yanqin Wang *

*Key Laboratory for Advanced Materials and Joint International Research Laboratory of Precision Chemistry and Molecular Engineering, Feringa Nobel Prize Scientist Joint Research Center, Research Institute of Industrial Catalysis, School of Chemistry and Molecular Engineering, East China University of Science and Technology, Shanghai 200237, China*

ARTICLE INFO

*Keywords:*
PVC upcycling
Cl transfer
Cl-containing chemicals
$Ru/Al_2O_3$ catalyst
Hydrogenolysis

ABSTRACT

The upcycling of waste polyvinyl chloride (PVC) is a grand challenge because of the unmanageable Cl species. Here, we develop a Cl-transfer strategy to upcycle waste PVC into value-added organic chlorides and PE-like polymer with various Cl acceptors (tetrahydrofuran, dibutyl ether and butanol) over $Ru/Al_2O_3$ catalyst. The high utilization efficiency of Cl (> 80 %) can be obtained over $Ru/Al_2O_3$ at 180 °C, 2Mpa $H_2$ with tetrahydrofuran as an acceptor within tens of hours. The excellent performance is attributed to key features including $Al_2O_3$ for the C-O bond activation and metal Ru for C-Cl bond activation and $H_2$ dissociation. The remaining PE-like polymer after removing Cl could be regarded as PE-like feedstock and further converted into methane through the same $Ru/Al_2O_3$ catalyst. The Cl-transfer system also enables the upcycling of several common PVC-contained wastes and works well in the scale-up test. This work offers a catalytic path to integrate waste PVC plastic into the supply chain of organic chlorides under the context of circular economy.

## 1. Introduction

Towards managing the dramatic increase in waste plastics since the 1950s, plastics recycling and upcycling are recognized to be promising options [1,2]. The key of plastic upcycling is to create an open–loop system whereby waste plastic can be reused and upcycled to value-added chemicals in sustainable manners [3]. Currently, recycling and upcycling of various plastics including polyethylene (PE), poly (dimethyl terephthalate) (PET), poly(lactic acid) (PLA), polyamides and polyethe, has been widely reported, but less attention was paid to the upcycling of polyvinyl chloride (PVC), which is the third most consumed commercial plastic [4]. The upgrading of PVC waste is one of the grand challenges for modern society owing to its disruptive impact on the environment.

PVC has a Cl content of up to 56 % and highly toxic Cl-containing compounds (e.g. dioxins) can be generated during common high-temperature degradations [5]. Moreover, these Cl-containing compounds can poison the active sites of catalysts due to the strong adsorption on metals. Therefore, compared to upcycling of other polyolefins such as PE and PP, PVC upcycling is more difficult due to its unmanageable Cl species. Common real plastic wastes are the mixtures containing PVC and still face the same problem and the treatment of the Cl-contained plastic mixtures is particularly important but very challenging. Traditionally, the treatment methods of waste PVC mainly include incineration, pyrolysis, hydrodechlorination and solvothermal carbonization [6]. However, these traditional methods have obvious drawbacks. Energy recovery by incineration is a common solution for most types of plastic wastes, but it poses a serious threat to the environment because that highly toxic dioxin and their derivatives are inevitably formed [7]. Pyrolysis requires high temperatures (>350 °C) and generates large amounts of corrosive HCl [8]. Although hydrodechlorination and solvothermal processes can remove Cl from PVC to inhibit the formation of dioxins, a large number of inorganic salts are inevitably formed, which increases the burden of post-processing and decreases the process economics [9–15]. Therefore, developing advanced technologies to upcycle PVC waste is extremely desirable.

Organic chlorides were widely used in modern industries, such as pharmaceuticals, methylcellulose, silicone resin manufacturing, agricultural chemicals, and other chemical processes [16]. Organic chlorides are usually produced by chlorination processes with toxic chlorinated reagents ($Cl_2$, $PCl_3$, etc.), raising major environmental concerns [17,18]. Developing environmentally benign and economically viable strategies to produce value-added organic chlorides is highly desirable. Waste PVC can be regarded as an abundant source of Cl,

* Corresponding authors.
*E-mail addresses:* jingyaxuan@mail.ecust.edu.cn (Y. Jing), wangyanqin@ecust.edu.cn (Y. Wang).

https://doi.org/10.1016/j.apcatb.2023.122671
Received 2 December 2022; Received in revised form 17 March 2023; Accepted 20 March 2023
Available online 23 March 2023

whose upcycling has been proposed only in electrochemical systems [19] but has been neglected in thermochemical treatment systems [6,8,20,21]. Conversion of waste PVC into Cl-containing chemicals can not only reduce PVC pollution but also provide promising routes to produce organic chlorides.

Here, we report a novel scheme of waste PVC upcycling via a Cl-transfer strategy that can transfer the Cl species into organic chlorides, leaving an easily manageable PE-like polymer, to integrate waste PVC into the production of organic chlorides (Fig. 1.), which can be used in the synthesis of relevant drugs (e.g. arylalkoxybenzamide derivatives [22], Phenylbutazone [23], etc.) or other chemicals (e.g. versatile ionic liquids [24], etc). and flame-retardant solvents [25]. We also demonstrated that the remaining PE-like polymer can be upcycled into methane through hydrogenolysis over $Ru/Al_2O_3$. The Cl-transfer strategy enables the conversion of various mixtures of PVC-containing waste plastics. $Ru/Al_2O_3$ showed the highest utilization efficiency of Cl (> 80 %) among the investigated catalysts in the Cl-transfer process. We explored the reaction network and catalytic mechanism of the Cl-transfer process and found that $Al_2O_3$ is responsible for the C-O activation and metal Ru enables the C-Cl activation and $H_2$ dissociation. We performed preliminary mass balance and prospected the technological process of the newly established system. To the best of our knowledge, in addition to unmanageable PVC, almost other C/O/N-containing plastics can be addressed through chemical upcycling ways. This work provides new ideas for PVC plastic upcycling.

## 2. Experimental section

### 2.1. Chemicals

$RuCl_3{\cdot}3H_2O$ was purchased from Aladdin Reagent Co., Ltd (Shanghai, China). Cerium nitrate hexahydrate was purchased from Aladdin Reagent Co., Ltd (Shanghai, China). PVC (k value is 65–68, Mw = 114,465) was purchased from Macklin Reagent Co., Ltd (Shanghai, China). n-Butanol was purchased from Aladdin Reagent Co., Ltd (Shanghai, China). Dibutyl ether was purchased from Aladdin Reagent Co., Ltd (Shanghai, China). Tetrahydrofuran was purchased from Aladdin Reagent Co., Ltd (Shanghai, China). Crotyl Chloride was purchased from Aladdin Reagent Co., Ltd (Shanghai, China). Commercial PVC sheets were purchased from the Odifu flagship store in taobao. The activated charcoal (>200 mesh) was purchased from Aladdin Reagent Co., Ltd (Shanghai, China). All purchased chemicals were analytical grade and used without further purification.

### 2.2. Catalyst preparation

$Al_2O_3$ was prepared by pseudo-boehmite calcination at 450 °C for 5 h in air. $CeO_2$ was prepared by calcination of cerium nitrate hexahydrate at 500 °C for 5 h in air.

$Ru/Al_2O_3$ was prepared by incipient wetness impregnation of $Al_2O_3$ with aqueous solutions of $RuCl_3$. After impregnation, the catalyst was dried at 60 °C for 12 h, followed by reduction in 10 % $H_2$ and 90 % Ar at 400 °C for 4 h. The $Ru/CeO_2$ and Ru/C catalysts were prepared by the same precursor of $Ru/Al_2O_3$. The real content of Ru was analyzed by ICP.

### 2.3. Catalyst characterizations

X-ray powder diffraction (XRD) patterns were recorded in the θ–2θ mode on a D8 Focus diffractometer (*CuKα1* radiation, k = 1.5406 Å), operated at 40 kV and 40 mA, respectively, within scattering angels of 10–80°. Transmission electron microscopy (TEM) images and EDS scanning of samples were obtained on a Talos F200X TEM at 200 kV. X-ray photoelectron spectroscopy (XPS) spectra were recorded on a Thermo Scientific Escalab 250 Xi system with monochromatic *Al Kα* radiation, and all results were calibrated using a C1s peak at 284.8 eV. To avoid the overlapping of peaks at around 285 eV of C1s and Ru3d, the Ru3p spectrum was chosen for the analysis.

The CO chemisorption of $Ru/Al_2O_3$ catalyst was recorded by using CO pulse chemisorption (VDsorb-91i automatic chemisorption instrument). The Ru dispersions were calculated based on the chemically adsorbed CO on the catalysts and the practical amount of Ru in the catalysts (CO: Ru = 1:1). All tests were carried out at ambient temperature. $H_2$-temperature-programmed reduction ($H_2$-TPR) profiles were measured by VDsorb-91i automatic chemisorption instrument. 100 mg sample was pretreated in Ar (30 mL/min) at 300 °C for 30 min and then cooled to room temperature. A reducing gas containing 10 % $H_2$/90 % Ar was employed at a flow rate of 30 mL/min and a heating rate of 10 °C/min from ambient temperature to 600 °C, using a TCD detector to monitor the $H_2$ consumption.

$H_2$-temperature-programmed desorption ($H_2$-TPD) profiles were also carried out on VDsorb-91i automatic chemisorption instrument. Typically, 100 mg sample was pretreated in Ar (30 mL/min) at 300 °C for 30 min and reduced by 10 % $H_2$/90 % Ar (30 mL/min) at 400 °C for 1 h. Subsequently, it was flushed with Ar (60 mL/min) at the same temperature for an hour and cooled to ambient temperature in the same gas flow. The sample was further saturated by 10 % $H_2$/90 % Ar (30 mL/min) for an hour at room temperature and flushed with Ar (30 mL/min) at the same temperature for 1 h to remove all the physisorbed hydrogen. The test sample was again heated from ambient temperature to 600 °C in Ar (30 mL/min) with a 10 °C/min heating rate. The $H_2$ concentration in the effluent gas was monitored by a TCD detector.

Solid $C^{13}$ NMR spectrum of residue solid on Brüker Advance 600 (Proton resonance frequency: 600.13 MHz Main magnetic field: 14.09 Tesla (superconducting)) at Shanghai Jiao Tong University Analysis and Testing Center.

Infrared (IR) spectra of pyridine adsorption were recorded on Nicolet NEXUS 670 FT–IR spectrometer. The samples were pressed into self-supporting disks and placed in an IR cell attached to a closed glass–circulation system. The disk was dehydrated by heating at 400 °C, for 1 h under vacuum to remove the physically adsorbed water. After the cell was cooled to room temperature, the IR spectrum was recorded as background. Pyridine vapor was then introduced into the cell at room–temperature until equilibrium was reached, and then a second

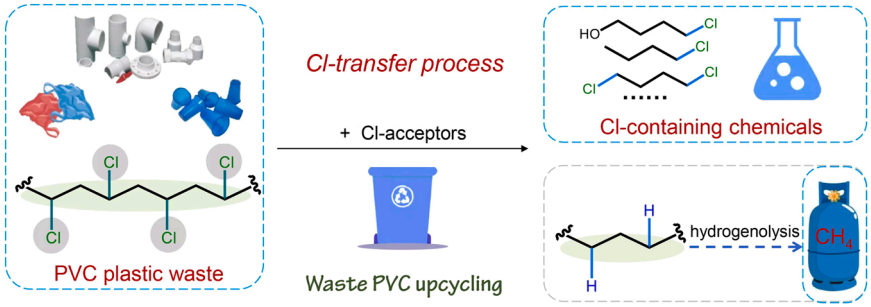


**Fig. 1.** The upgrading of waste PVC into organic chlorides stream via Cl-transfer system.

spectrum was recorded. The subsequent evacuation was performed at 100 °C, for 10 min followed by spectral acquisitions. The spectra presented were obtained by subtracting the spectra recorded before and after pyridine adsorption.

Diffuse reflectance infrared Fourier transform spectra (DRIFTS) of dichlorobutane (DCB)-adsorption were recorded on Nicolet Model iS-50 FT-IR spectrometer equipped with an MCT/A detector. The FT-IR spectra were recorded with a resolution of 4 $cm^{-1}$ and 32 scans. Before the experiment, the samples were in-situ reduced by 10 % $H_2$/90 % Ar for 1 h at 400 °C and cooled down to room temperature and background spectra were recorded at 30 °C. Then DCB with Ar was bubbled into the in situ cell for 40 min and the physical adsorption of DCB were recorded. Next, the cell was purged with Ar at 30 °C for 30 min and the chemisorption spectra of DCB were recorded.

Diffuse reflectance infrared Fourier transform spectrum (DRIFTS) of tetrahydrofuran (THF)-adsorption was recorded on Nicolet Model iS-50 FT-IR spectrometer equipped with an MCT/A detector. The FT-IR spectra were recorded with a resolution of 4 $cm^{-1}$ and 32 scans. Before the experiment, the samples were in-situ reduced by 10 % $H_2$/90 % Ar for 1 h at 400 °C and cooled down to room temperature and background spectra were recorded at 30 °C. Then THF with Ar was bubbled into the in situ cell for 40 min and the physical adsorption of THF were recorded. Next, the cell was purged with Ar at 30 °C for 30 min and the chemisorption spectra of THF were recorded.

*In situ* IR spectra were also recorded on Nicolet Model iS-50 FT-IR spectrometer equipped with an MCT/A detector. The FT-IR spectra were recorded with a resolution of 4 $cm^{-1}$ and 32 scans. Before the experiment, the pre-reduced catalyst ($Ru/Al_2O_3$) is fully mixed with PVC and filled into the in-situ cell. The procedure follows the three steps: 1) the sample was pretreated by Ar for 1 h at 120 °C and then increased the reaction temperature to 180 °C and the background spectrum was recorded; 2) THF was bubbled into the in situ cell for 30 min to make the sample fully adsorb THF and then the cell was purged with Ar (180 °C for 30 min) and the spectrum was recorded as 'the initial spectrum of the reaction'; 3) THF in Ar stream was again bubbled into the cell for 120 min and after removing physically adsorbed THF, the IR spectrum of sample was recorded as the 'after THF treatment without $H_2$'. The first difference spectrum obtained by subtracting "the initial spectrum of the reaction" is recorded as 'Diff-THF without $H_2$'; 4) THF in 10 % $H_2$/90 % Ar stream was bubbled into the cell for 120 min and after removing physically adsorbed THF, the IR spectrum of sample was recorded as the 'after THF treatment in $H_2$'. The second difference spectrum obtained by subtracting the initial spectrum of the reaction is recorded as 'Diff-THF in $H_2$'.

*In situ* temperature-programmed desorption of dichloromethane by mass spectrometry (DCM-TPD-MS) was performed on a Huasi DAS-7200 automatic chemisorption instrument. Before analysis, the catalysts (100 mg) were pretreated in the cell in Ar at 400 °C for 30 min, followed by cooling to room temperature in pure Ar. Then, the dichloromethane molecule was physically mixed with the reduced catalyst and added into a quartz tube together. The tested sample was then heated to 400 °C with a heating rate of 5 °C/min under a 30 mL/min Ar flow. Fragment signals were recorded with a Linglu mass spectrometer that was directly connected to the outlet of the reaction tube.

### 2.4. Catalytic test of Cl-transfer process and product analysis

The detailed reaction conditions are described in the Fig. captions and table footnotes. In a typical reaction with PVC conversion as an example, catalyst (0.1 g), PVC (0.1 g) and THF (5 g) were loaded into a stainless-steel autoclave reactor. After the reactor was purged with $H_2$ three times and charged to the target $H_2$ pressure (2 MPa), the reaction was conducted at the target temperature (180 °C) with a magnetic stirring speed of 600 r.p.m. After the reaction, the reactor was quenched to ambient temperature in an ice-water bath. After cooling, 5 mL MeOH was added to precipitate the unreacted PVC and 100 μl pentadecane (internal standard) was added and stirred for 10 min to ensure that the pentadecane was completely dispersed. Then, the liquid solution was separated from the solid catalyst and unreacted PVC by centrifugation and was directly analyzed by gas chromatography (GC) and GC–MS on an Agilent 7890B gas chromatograph with a flame ionization detector and an Agilent 7890 A GC-MS instrument, both equipped with HP-5 capillary columns (30 m * 250 mm).

The yield of products was calculated by using the equation:

$$\text{Yield} = (\text{mole of products})/(\text{mole of Cl in PVC}) \times 100\ \%.$$

The production distribution in the liquid phase was calculated by using the equation:

$$\text{Production distribution} = \text{Y (product)}/(\text{total yield}) \times 100\ \%.$$

The utilization efficiency of Cl was determined by the following equation:

$$\text{Yield (Cl)} = (\text{sum Cl mole of all organic product})/(\text{mole of Cl in PVC}) \times 100\ \%.$$

After the Cl-transfer reaction, the isolated solid was dispersed in deionized water to separate unreacted polymers (residue) and catalysts because the polymer can float on the surface while the catalyst sinks under the bottom. To remove the $Cl^-$ ions adsorbed on residues, the residue was washed 3 times with 5 mL water and 5 mL methanol, respectively. Next, the residue was collected after drying in 60 °C vacuum oven.

The chloride content in the residue was determined by using a chloride ion selective electrode. The measurement procedure includes: (1) the residue (0.1 g) was hydrothermally treated for 12 h with 1 M NaOH solution (60 mL) under 200 °C to remove Cl from the residue [26]; (2) solid and liquid were separated by centrifugation; (3) the liquid was diluted to 500 mL with deionized water; (4) The content of Cl in the residue is obtained by measuring the mass concentration of $Cl^-$ in the liquid with a chloride ion selective electrode. The Cl content in the residue is calculated by the following equation:

$$\text{The Cl content} = (\text{the mass concentration of } Cl^- \times 500)/\text{ the mass of residue} \times 100\ \%.$$

The Cl content in PVC-contained materials (common PVC sheet and post-consumer PVC materials) was also measured with the same procedure.

### 2.5. Catalytic test of the residue hydrogenolysis

Typically, residue (0.2 g) and $Ru/Al_2O_3$ catalyst (0.1 g) were loaded into a stainless-steel autoclave reactor. After the reactor was purged with $H_2$ three times and charged to the target $H_2$ pressure (3 MPa), the reaction was conducted at the target temperature (350 °C). After the reaction (8 h), the reactor was quenched to ambient temperature in an ice-water bath. After cooling, the temperature and press were measured and the gas was collected into an aluminum foil gas collecting bag for gaseous products analysis with gas chromatography (GC2060) [flame ionization detector, equipped with $Al_2O_3/Na_2SO_4$ capillary columns (30 m * 0.32 mm*10 μm)]. Then, 400 μl mesitylene and 3 mL *p*-xylene were added into the reactor and stirred for 10 min to ensure that the mesitylene was completely dispersed and the products were fully dissolved in *p*-xylene. After centrifugation, the liquid products were analyzed by gas chromatography (GC) and GC–MS on an Agilent 7890B gas chromatograph with a flame ionization detector and an Agilent 7890A GC-MS instrument, both equipped with HP-5 capillary columns (30 m * 250 mm). Mesitylene was used as an internal standard for the quantification of liquid products and the gas products were quantitated by an external standard method.

The carbon yield of residue conversion was calculated by using the following equation:

Yield (Y) = (sum mole of C in all products)/(mole of C in residue) × 100 %.

## 3. Results and discussion

### 3.1. The designed Cl-transfer system

The key of the Cl-transfer process is to accept Cl in PVC with nucleophilic reagents. First, several common nucleophilic reagents including tetrahydrofuran (THF), butyl alcohol (BuOH) and butyl ether (DBE) were employed as the acceptors of Cl to perform the designed Cl-transfer system (Fig. 2a). All investigated acceptors have the ability to perform the Cl-transfer process and THF afforded the highest utilization efficiency of Cl (56.3 %) with 1 or 2-Cl containing products. The ability to capture Cl follows the sequence: THF > DBE > BuOH, which may be related to the dissociation energy of their C-O bonds [27] and their solubility (Fig. S3) for PVC. Noteworthy, the single 1-chlorobutane product was obtained when DBE or BuOH as the Cl acceptor despite their low utilization efficiency of Cl, highlighting their potential to selectively produce the single product. After optimizing reaction conditions, the considerable utilization efficiency of Cl (>40 %) was also achieved while still keeping the simple product when DBE or BuOH as the Cl acceptor. And, we also examined the effect of the PVC to Cl acceptor (THF) mass ratio (Table S1). The utilization efficiency of Cl gradually increased with the decrease of the ratio from 1/1–1/25. When the ratio was further reduced to 1/50, the utilization efficiency of Cl remained unchanged. Thus, the mass ratio lower than 1/25 allows the two roles to work well. To simplify the reaction system as much as possible, we use the Cl acceptor molecule as single solvent. In short, with Cl receptors as solvents, this strategy can smoothly transfer the unmanageable Cl species from PVC to Cl acceptors to obtain value-added Cl-containing chemicals, even a single product.

We performed an optimization of the reaction conditions using THF as the chloride acceptor (Fig. S1). When the $H_2$ pressure increased from 0.6 to 2 MPa, the utilization efficiency of Cl increased from 32.7 % to 56.3 %. While further increasing to 4.2 MPa, the Cl utilization efficiency has no obvious change. Yield and product distribution versus reaction temperature show that lower temperature (160 °C) leads to a low Cl utilization efficiency (12.6 %), whereas higher temperature (200 °C) favors PVC pyrolysis dichlorination (Fig. S2), which produces more undesired corrosive HCl. In short, the reaction at 180 °C under 2 MPa is the optimal reaction condition.

Then, THF was selected as the acceptor to investigate the conversion of PVC over various catalysts (Fig. 2a). Generally, the C-Cl activation of

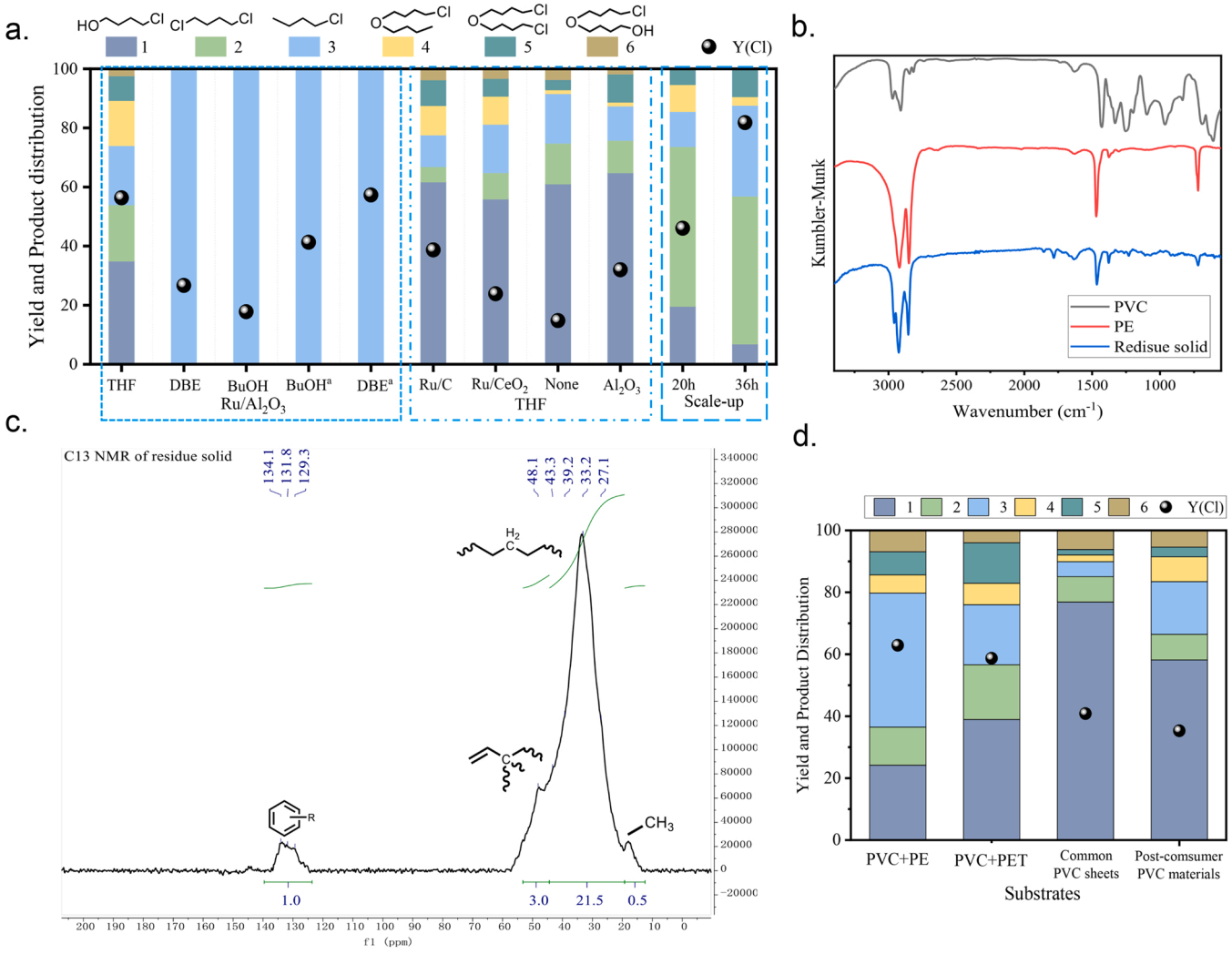


**Fig. 2.** (a) Comparison of catalytic performance of different catalysts. Conditions: 0.1 g PVC, 0.1 g catalyst, 5 g THF, 180 °C, 2 MPa $H_2$, 10 h; [a] 0.1 g PVC, 0.1 g Catalyst, 5 g Cl-acceptor (BuOH or DBE), 180 °C, 2 MPa $H_2$, 20 h; The conditions of scale-up tests: 2.5 g PVC, 0.1 g Catalyst, 5 g THF, 180 °C, 2 MPa $H_2$; (b) The IR spectra of PVC (black), PE (red), residue solid after reaction (blue); (c) Solid State $C^{13}$ NMR spectra of residue solid; (d)The utilization efficiency of Cl for PVC-containing substrates. Conditions: 0.1 g substrate, 0.1 g $Ru/Al_2O_3$, 5 g THF, 180 °C, 2 MPa $H_2$, 20 h.

organochloride occurs on metal sites, such as Pd, Pt and Ru [28–32]. We also performed a screening of catalyst metals (Table S2), and Ru has higher activity compared to the metal Ni, and similar activity compared to the metal Pd. Besides, metal Ru has excellent resistance to Cl toxicity [33] and a lower cost. Moreover, Ru-based catalysts are also active in the hydrodechlorination and hydrogenolysis reactions [34,35]. Therefore, Ru is the best candidate for the next investigation and several common supported Ru catalysts were tested and the results were shown in Fig. 2a. Among these, $Ru/Al_2O_3$ gave the highest yield (56.3 %) of organic chlorides. Low yields (14.8 % and 32.0 %) were obtained in catalyst-free and pure $Al_2O_3$ conditions, respectively. These results indicate that the reaction can occur efficiently on the multifunctional $Ru/Al_2O_3$ catalyst. Furthermore, the yields over Ru/C (36.1 %) and $Ru/CeO_2$ (23.9 %) were markedly lower than that over $Ru/Al_2O_3$, suggesting that besides metal Ru sites, the acidic sites also play an important role in the Cl-transfer process. In short, $Ru/Al_2O_3$ is the most active catalyst for the transfer of Cl from PVC into organic chlorides.

The above results confirm that the designed reaction indeed achieves the goal of transferring Cl species of PVC into organic chlorides with common nucleophilic reagents as Cl acceptors over $Ru/Al_2O_3$. The residual solid was characterized by thermogravimetry (Fig. S4), the results show that the thermogravimetric curves of the residual solids are very close to those of PE, while they show great differences with PVC, indicating that the solid residues have a high similarity with PE. Then, the focus is to explore the structure of the residue solid after removing Cl species from PVC. IR spectrum of the residue solid was recorded and the results (Fig. 2b) show that the spectrum of the residue solid after the reaction was highly similar to that of pure PE at the region of 2800–2900 $cm^{-1}$, 1480 $cm^{-1}$ and 710 $cm^{-1}$ attributed to the stretching mode of C-H bond, the stretching mode of C-C bond and the characteristic mode of multiple -$CH_2$- repeating units respectively. However, no signals attributed to C–Cl stretching vibration (606 $cm^{-1}$) and other vibration signals affected by Cl such as -$CH_2$ deformation vibration (900–1400 $cm^{-1}$) and alkane C–H stretching vibration (2800–2900 $cm^{-1}$) were observed, indicating that Cl species were removed almost completely and the structure of residue solid is very similar with that of PE. The solid NMR $C^{13}$ spectrum of residue solid was also characterized. As shown in Fig. 2c, the signals at 10–50 ppm are generally classified as the signal in the saturated carbon chain including CH3, CH2, -CH- etc [36]. The peaks at 120–130 ppm are classified as $C^{13}$ signals in C═C. In the obtained spectrum, the signals mainly lie at 20–50 ppm and very few signals are found at 120–130 ppm, indicating that in the solid residue, most of C species present a form of saturated carbon chains, which is consistent with the IR characterization results. The peaks attributed to $C^{13}$ signals in -CHCl- should lie at 60–70 ppm and are not obvious [37]. These results confirm that the solid residue has a similar structure with PE and extremely low Cl residuals.

Considering that the residue solid and PE share substantial structural similarities, we tried to degrade the residue solid by adopting similar approaches of PE upcycling. PE is the most consumed plastic and towards PE upcycling, many advanced technologies emerged and hydrogenolysis on metal-supported catalysts is arguably the most successful strategy to degrade waste PE [38,39]. In particular, the acidic sites and Ru metal sites may cause by hydrogenolysis PE to produce methane gas, which is one of the cleanest fuels and is in increasing demand [40–42]. Inspired by this, we tested the hydrogenolysis of the residue solid over $Ru/Al_2O_3$ at 350 °C and encouragingly obtained a 91.8 % yield of methane, indicating that the residue solid can be easily upcycled as the process of PE upcycling. Considering the possible presence of Cl in the system, the Cl poisoning effect under this condition was also explored. As shown in Fig. S5, the used catalyst can also give a high yield of methane (92.2 %) comparable to fresh catalyst (91.8 %) in the hydrogenolysis of solid residues when the Cl transfer is not complete, indicating that the catalyst is insensitive to Cl poisoning at 350 °C, probably because the high temperature favors the desorption of Cl species from Ru surface. However, Chen et al. investigated the effect of the presence of PVC on Ru-catalyzed hydrogenolysis, which exhibited a strong detrimental effect on catalyst activity at 225 °C [43]. The difference of poisoning effect between the above work and our system may be caused by the different temperature range.

Based on the above results, we here describe the designed Cl-transfer system: the Cl species in PVC is transferred to value-added Cl-contained chemicals with common nucleophilic reagents as Cl acceptors over $Ru/Al_2O_3$, while the remaining solids are highly structurally similar to PE. Then, the residue solid can be converted using emerging technologies of PE upcycling and we demonstrated a successful example of hydrogenolysis to methane.

Furthermore, we conducted a scale-up experiment of 25 times more than the original PVC mass (2.5 g). After optimizing the conditions, the utilization efficiency of Cl reaches up to 81.8 %, suggesting its great potential for scale-up applications. Our ultimate objective is to convert real PVC-containing waste plastics via the advanced Cl-transfer process. Hence, after a preliminary analysis of the composition of these materials (Table S3), the direct conversion of various PVC-containing wastes including a mixture of PE and PVC (mass ratio is 1/1), a mixture of PET and PVC (mass ratio is 1/1), common PVC-contained sheet (Cl content is 5.9 %) and post-consumer PVC-contained materials (Cl content is 16.4 %) were tested to investigate the applicability of our newly established system. The results (Fig. 2c) show that all samples could be converted in considerable utilization efficiencies of Cl, demonstrating that our system can handle common PVC-containing plastic mixtures. The following focus is placed on the exploration of the Cl-transfer pathway and the catalytic mechanism over $Ru/Al_2O_3$.

### 3.2. The Cl-transfer pathway studies

To explore the reaction pathway over $Ru/Al_2O_3$, yield versus reaction time was investigated (Fig. 3a). Firstly, the chlorobutanol (compound 1) was formed in the initial reaction with 14.2 % yield, while the yield of other products is extremely low, indicating that Cl is first transferred from PVC to compound 1. Further, compound 1 is converted through three possible pathways: i) chlorination to dichlorobutane (compound 2), ii) hydrogenolysis to chlorobutane (compound 3), iii) self-etherification or etherification with other intermediates to 1-butoxy-4-chlorobutane (compound 4), 4,4-dichlorobutyl ether (compound 5) and 4-(4-chlorobutoxy)butan-1-ol (compound 6) and compound 4 may also be obtained by hydrogenolysis of compound 5 and compound 6, respectively (Fig. 3b). Moreover, as the reaction time increases, the yield of compound **1** increases firstly and then decreases, suggesting that the Cl-transfer occurs mainly between PVC and THF, instead of between Cl-containing molecules. Furthermore, when keeping the utilization efficiency of Cl be almost the same (Fig. S6), slightly different product distributions were observed over various catalysts. The major findings include that Ru-based catalysts gave more hydrogenolysis products because of Ru for the dissociation of $H_2$ and acid sites favor the deep chlorination due to Lewis acid for the C-O activation. Thus, we speculate that Ru is mainly responsible for the dissociation of $H_2$ and the activation of C-Cl, while the acidic sites on $Al_2O_3$ mainly favor in the activation of oxygenated substrates, which is important in the Cl transfer and etherification. Overall the utilization efficiency of Cl considerably increases from 19.7 % to 63.9 % as the time prolongs from 1 to 15 h. However, further extension of reaction time results in its decrease due to the excessive hydrochlorination, implying that 15 h is an appropriate time for the Cl-transfer process. To better understand excessive hydrodechlorination, HCl was employed as a substrate in place of PVC (Table S4), while the utilization efficiency of Cl (31.56 %) was lower than that with PVC as a substrate, demonstrating that HCl could also partly react with THF back to organic chlorine via compound 1 over $Ru/Al_2O_3$.

It should be noted that the utilization efficiency of Cl is less than 100 %. To explore the reason for the utilization efficiency of Cl less than 100 %, the Cl equilibrium of the sample with 10 h of reaction was examined

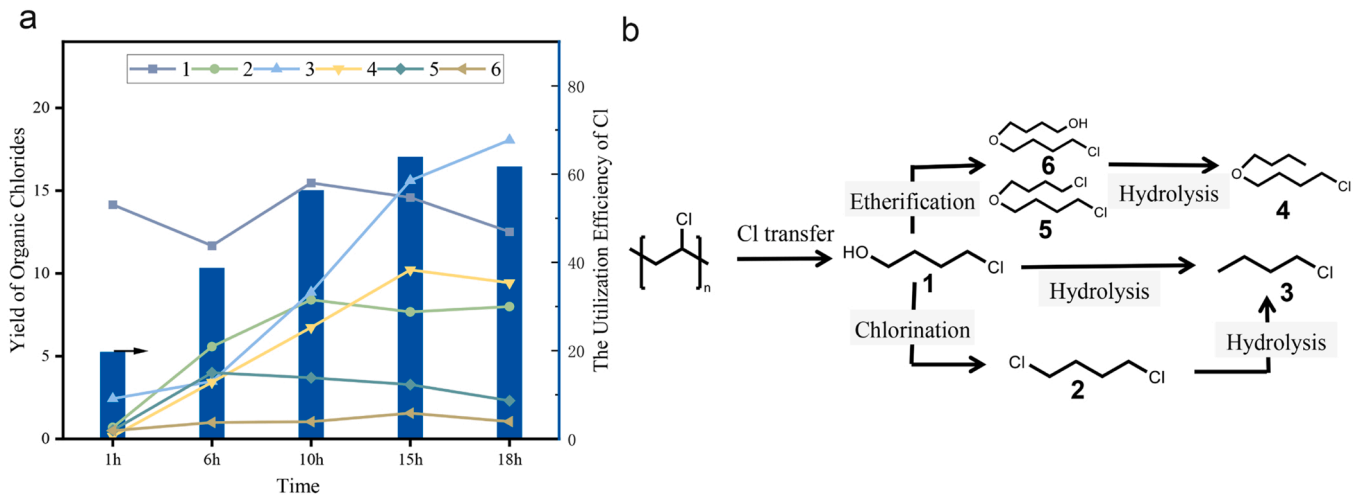


**Fig. 3.** (a) The results of yield versus reaction time over $Ru/Al_2O_3$. Conditions: 0.1 g PVC, 0.1 g $Ru/Al_2O_3$, 5 g THF, 180 °C, 2 MPa $H_2$; (b) Proposed Cl-transfer reaction pathway.

(Table S5). Firstly, the gas after the reaction was slowly passed through 0.1 M NaOH solution to absorb the potential HCl and found that the pH had no change, suggesting very little loss in the gas. Secondly, the solid after the reaction was hydrothermally treated to measure the $Cl^-$ content and 18.2 % Cl content (based on PVC) was obtained. Finally, the liquid after the reaction was hydrothermally treated and 71.2 % Cl content (based on PVC) was obtained. Consequently, there is still ~10 % of Cl loss, probably because of the adsorption of Cl-containing molecules on the catalyst surface and inevitable loss in the operation process. In addition, we also directly measured the $Cl^-$ content in liquid without hydrothermal treatment and found that the contents of inorganic and organic Cl species are 11.6 % and 56.3 %, respectively. The sum of two (67.9 %) is lower than 71.2 %, indicating that a small number of Cl-containing products in the organic phase probably cannot be detected by GC.

### 3.3. The catalytic mechanism of Cl-transfer reaction

#### 3.3.1. Characterizations of $Ru/Al_2O_3$

Various characterizations were conducted to reveal the structure and property of $Ru/Al_2O_3$ (Fig. 4). $NH_3$-TPD of $Al_2O_3$ (Fig. 4a) shows an obvious desorption signal at 200–400 °C, suggesting abundant medium-strong acid sites on $Al_2O_3$. To clarify the role of acidity, Ru/C was also characterized by $NH_3$-TPD (Fig. S7L), which only had an extremely weak peak in the range of 100–200 °C, confirming that the acidity favors the reaction. Py-FTIR characterization of $Al_2O_3$ was performed in Fig. S7R, which showed a significant peak only at 1450 $cm^{-1}$, indicating that the acidic site of the catalyst is mainly Lewis acid. The XRD pattern (Fig. 4b) illustrates that the broad diffraction peak corresponding to γ-$Al_2O_3$ was observed on $Ru/Al_2O_3$, indicating a large number of amorphous structures of γ-$Al_2O_3$. No clear Ru diffraction peak was observed, presumably due to its small size and good dispersion, which is also confirmed by STEM images (Fig. 4d). HAADF-STEM (Fig. 4d) gave visual Ru particles and a wide distribution of Ru particle size. Moreover, the estimated particle size of Ru was 2.9 nm by the empirical formula of dispersion-grain size combined with CO-DRIFT results of $Ru/Al_2O_3$ (Fig. S8 and Fig. 4f), which is close to the STEM statistic result (2.4 nm). Considering the errors of both methods, an average value (2.7 nm) was confirmed to be the particle size of Ru.

The $H_2$-TPR measurement (Fig. 4c) shows two reduction peaks of $Ru/Al_2O_3$, which can be assigned to the reduction of chlorinated Ru (90 °C) and RuO species (156 °C), respectively [44,45]. The chemical states of Ru species were characterized by XPS. The $Ru^0$ is characterized by the $Ru3p_{3/2}$ peak at 462.3 eV and $Ru3p_{1/2}$ peak at 484.5 eV whereas $Ru^+$ is characterized by two peaks at 463.7 eV and 486.2 eV [46]. As shown in Fig. 4e, only $Ru^0$ species were found over $Ru/Al_2O_3$. The hydrogen release amount of $Ru/Al_2O_3$ was also measured (Fig. 4f), and the released 22.7 μmol/g $H_2$ was detected, indicating that $Ru^0$ species are responsible for the $H_2$ activation.

In short, the above results confirm that $Ru/Al_2O_3$ has highly dispersed $Ru^0$ sites and abundant acid sites. A convincing consensus is that Lewis acid sites favor the activation of C-O bonds in the hydrogenolysis of oxygenated compounds and metallic state species enable the dissociation of $H_2$ [47,48]. It is therefore reasonable to believe that Lewis acid sites of $Al_2O_3$ and $Ru^0$ sites are responsible for the activation of C-O bonds in Cl acceptors and the corresponding intermediate and the dissociation of $H_2$, respectively. The remaining question is which species is the dominant active site for the activation of C-Cl bonds in PVC.

#### 3.3.2. The catalytic mechanism of C-Cl activation over $Ru/Al_2O_3$

To verify the C-Cl activation over $Ru/Al_2O_3$, dichlorobutane was employed to perform adsorption-desorption DRIFTS experiments (Fig. 5a). The peak at 2873 $cm^{-1}$ is attributed to C-H stretching vibration in -CHCl- group of dichlorobutane (DCB) [49,50]. A clear blue shift at 2881 $cm^{-1}$ ($\Delta = 8$ $cm^{-1}$) was observed over $Ru/Al_2O_3$, but only 4 $cm^{-1}$ shift was found over $Al_2O_3$, indicating that the strong adsorption-activation to the C-Cl bonds shortens the C-H bonds over Ru species, leading to stronger C-H vibrations. Besides, the TPD-MS experiments of $CH_2Cl_2$ were performed under Ar atmosphere (Fig. 5b). The result shows a clear signal of $CH_2Cl_2$ desorption on $Ru/Al_2O_3$, but no similar signal on $Al_2O_3$, again confirming that Ru species is the main sites of C-Cl adsorption-activation, in agreement with DCB-DRIFTS. Those results confirm that Ru is the main active site for the C-Cl activation and $Al_2O_3$ has no obvious contribution in this piece.

Next, to verify the C-O activation over $Ru/Al_2O_3$, THF was employed to perform adsorption-desorption DRIFTS experiments (Fig. S9). The peaks at 1082 $cm^{-1}$ and 2870 $cm^{-1}$ are attributed to C-O stretching vibration and C-H stretching vibration in -CH-O-CH- group of THF [51], respectively. The same spectra for $Al_2O_3$ and $Ru/Al_2O_3$ confirm that the primary adsorption sites reside on $Al_2O_3$ and Ru has little effect on the adsorption of THF. Compared with the physical adsorption over $Al_2O_3$, a clear red shift at 1082 $cm^{-1}$ ($\Delta = 11$ $cm^{-1}$) and a blue shift at 2870 $cm^{-1}$($\Delta = 8$ $cm^{-1}$) were observed over $Al_2O_3$, suggesting that the strong adsorption-activation of the C-O bonds. In short, the results confirm that $Al_2O_3$ is the main active site for the C-O activation and Ru has no obvious contribution.

Then, in situ IR was used to monitor the structural changes of PVC without $H_2$ or in $H_2$ and the IR differential spectra were obtained by

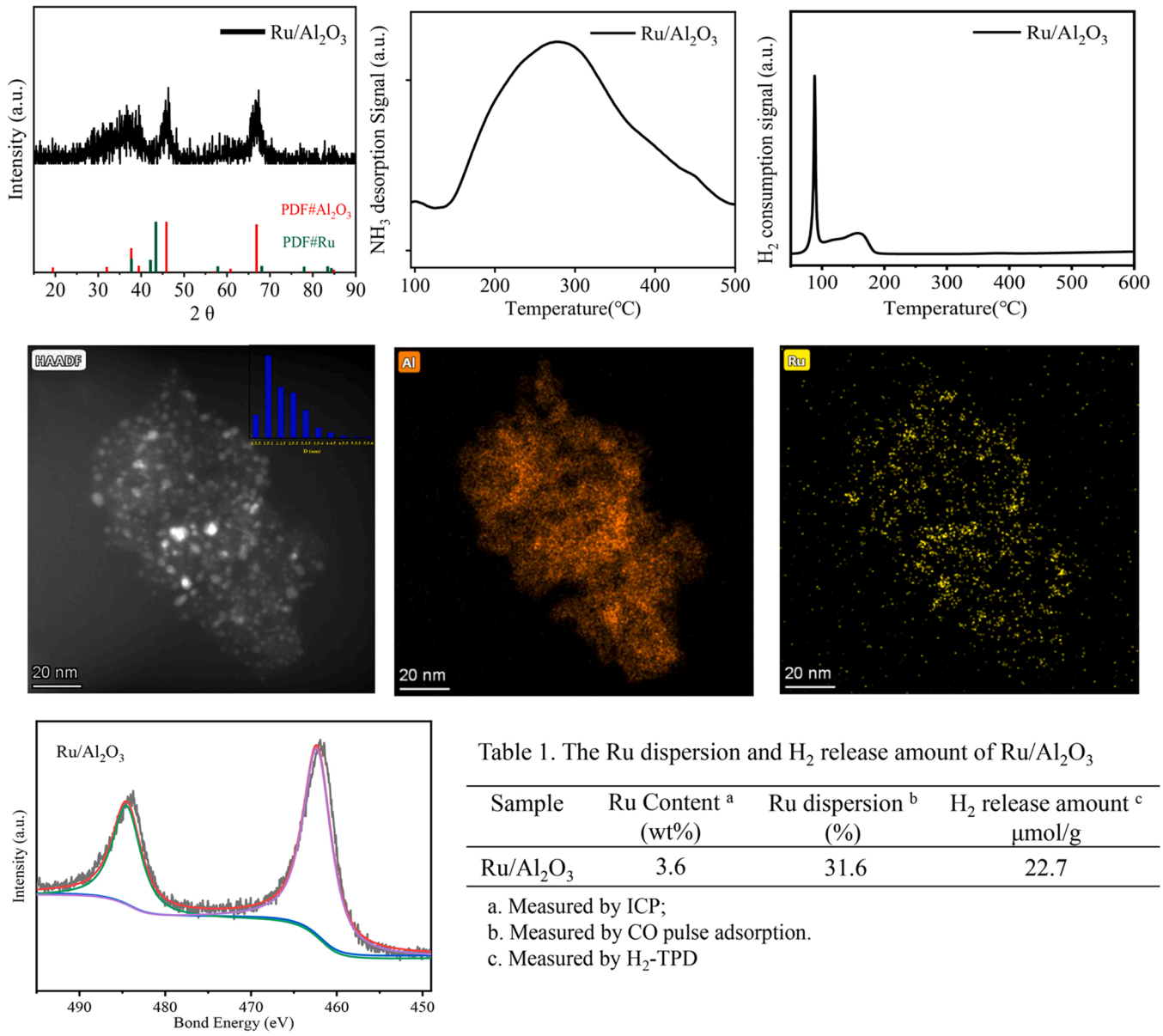


Table 1. The Ru dispersion and $H_2$ release amount of $Ru/Al_2O_3$

| Sample | Ru Content [a] (wt%) | Ru dispersion [b] (%) | $H_2$ release amount [c] μmol/g |
|---|---|---|---|
| $Ru/Al_2O_3$ | 3.6 | 31.6 | 22.7 |

a. Measured by ICP;
b. Measured by CO pulse adsorption.
c. Measured by $H_2$-TPD

**Fig. 4.** Characterization of $Ru/Al_2O_3$ catalyst. a), $NH_3$-TPD profile. b), XRD pattern; c), $H_2$-TPR profile; d), HAADF-STEM and EDS maps; e), XPS spectrum; f), The Ru dispersion and $H_2$ release amount.

subtracting the spectra before and after the treatment. As shown in Fig. 5c, after THF treatment without $H_2$ (black line), significant peaks at 1000–1100 $cm^{-1}$ ascribing to the stretching mode of C-O bond were observed [52,53], directly illustrating that C-O bond was formed in PVC during the reaction. Meanwhile, the peaks at 1200–1500 $cm^{-1}$ corresponding to the stretching mode of C-C bond in -C-CX (X = H, O, Cl), the peaks at 3000–3100 $cm^{-1}$ corresponding to the stretching mode of C-H bond in $-CH_2-$ group of THF alkyl chain and 3200–3300 $cm^{-1}$ corresponding to the stretching mode of hydrogen bond were also observed, also confirming the connection of O atom in THF and C atom in PVC after removing Cl species. In addition, the peaks at 2900–3000 $cm^{-1}$ and 1500–1700 $cm^{-1}$ corresponding to the stretching mode of C-H bond in -C═CH and the stretching mode of C═C bond respectively were found, probably because a part of PVC undergoes the direct elimination of C-Cl bond in this process. Moreover, the IR differential spectrum after THF treatment in $H_2$ was also obtained (Fig. 5c, red line), Compared to the spectrum without hydrogen, all peaks are significantly weaker, which indicates that most species are converted and desorbed within $H_2$. Especially, the peaks at 1000–1100 $cm^{-1}$ attributing to the C-O stretching vibration signal are significantly reduced, meanwhile the signal around 3200 $cm^{-1}$ attributing to hydrogen bonding also disappears, suggesting that the C-O hydrogenolysis occurs under $H_2$ atmosphere. In conclusion, the changes in the in situ IR signal are consistent with the direct grafting of THF onto PVC and its subsequent hydrogenolysis in the presence of hydrogen, suggesting that the transfer of Cl between PVC and THF occurs directly through a substitution-hydrogenolysis mechanism.

As mentioned before, when HCl in place of PVC is the substrate, the HCl-involved Cl-transfer mechanism indeed occurs, i.e. HCl is formed first from PVC, which initiates the reaction with THF. Therefore, the direct Cl-transfer mechanism and HCl-involved Cl-transfer mechanism could co-exist. However, based on previous reports [54,55], the hydrogenation of C═C bonds is hard to occur in the presence of Cl species, because the hydrogenation ability of Ru could be inhibited by Cl species. To verify this point, PVC was partially dechlorinated through the pretreatment in 1 M NaOH (a.q.) at 120 °C for 5 h to generate C═C bonds, and then the obtained PVC with C═C bonds was used as a substrate to test its hydrogenation of C═C bonds. As shown in Fig. S11, the ratio of

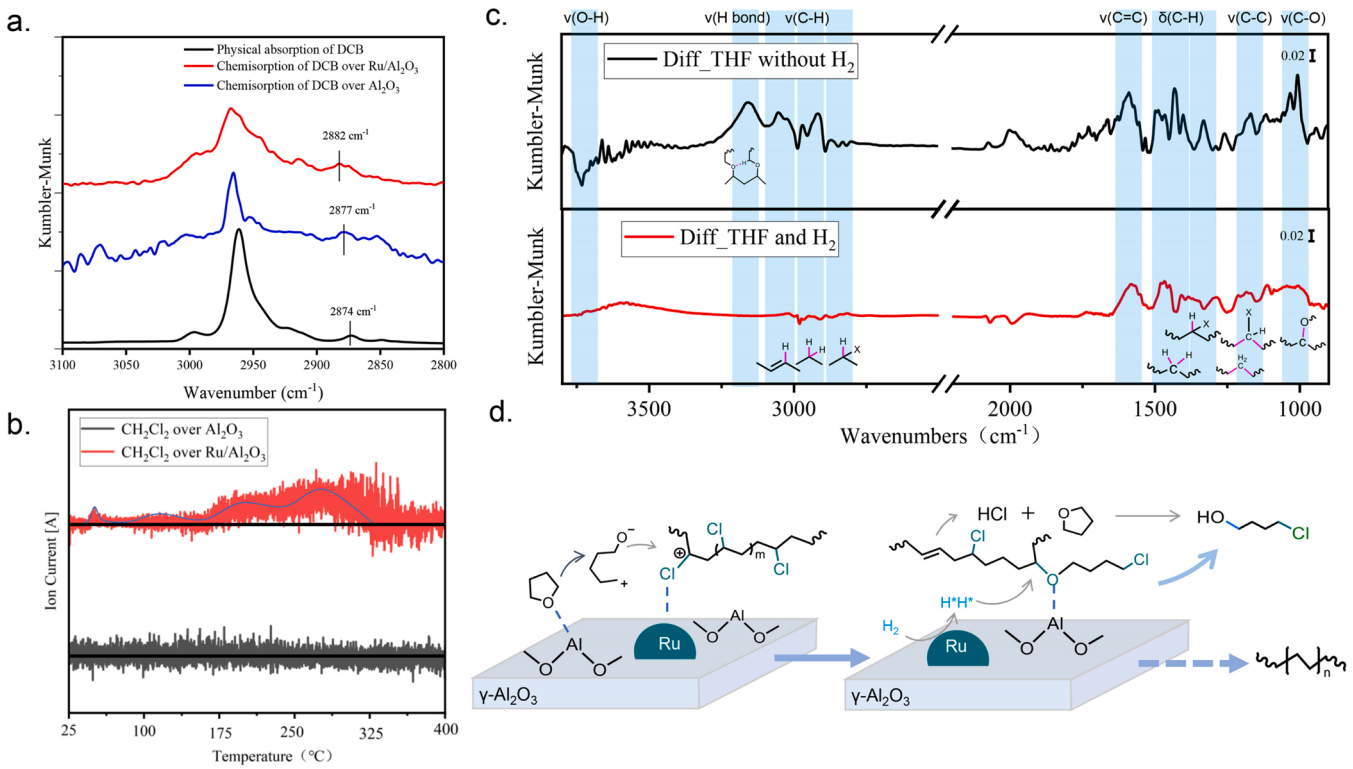


**Fig. 5.** (a) in situ DRIFTS spectra of 1,4-dichlorobutane over $Ru/Al_2O_3$; (b) DCM-TPD-MS profiles over $Ru/Al_2O_3$ and $Al_2O_3$; (c) *In situ* IR difference spectra in different treatment procedures; (d) The possible catalytic mechanism of Cl-transfer reaction.

C═C bonds has no obvious reduction, indicating that the C═C bonds cannot be smoothly hydrogenated due to the presence of Cl species. Moreover, new signals ascribed to the C═C bonds of aromatic ring appeared, further suggesting that the substrate tends to polymerization/aromatization, instead of hydrogenation of C═C bonds. These results indicate that the hydrogenation of generated C═C bonds through dichlorination is difficult. Therefore, combining the $C^{13}$ signal contributing to C═C structure in the residue solid ($C^{13}$ NMR) is very weak, this process mainly follows the substitution-hydrogenolysis mechanism.

Based on the above results, we propose a possible mainly catalytic mechanism of Cl-transfer reaction (Fig. 5c): Firstly, THF ring is activated by Lewis acid sites of $Al_2O_3$, resulting in the ring opening to generate a carbocation and an alkoxide anion. Meanwhile, C-Cl bond is mainly activated by Ru metal sites [56–59]. Then a non-catalytic nucleophilic substitution occurs to form a polymer intermediate, that is, the carbocation accepts Cl and the alkoxide anion grafts on PVC [60]. Next, the C-O bond of the polymer intermediate is cleaved through hydrogenolysis, where Lewis acid sites of $Al_2O_3$ and metal Ru sites are responsible for the activation of C-O bond and hydrogen, respectively. Finally, chlorobutanol desorbs from the catalyst's surface and a PE-like polymer is gradually formed. In short, the multifunctional $Ru/Al_2O_3$ catalyst plays key roles including: 1) Lewis acid sites for the C-O activation; 2) metal Ru for the C-Cl activation and $H_2$ dissociation.

### 3.4. Comparation of Cl-transfer and traditional systems and mass balance

At present, the treatment procedure (Fig. 6a) of plastic mixtures containing PVC includes that: 1) the plastic mixture is collected at the waste treatment plant, 2) PVC is removed from plastic mixtures by sorting or other separation techniques because traditional processes are not compatible with PVC, 3) the remaining plastic mixtures are upcycled through the existing mature methods such as incineration, pyrolysis, catalytic hydrogenolysis, etc. However, the sorting process causes expensive costs and shows very limited efficiency due to the complex structure and composition of plastic mixtures. Meanwhile, the conversion of the obtained PVC through separating also remained a big challenge. Our newly established Cl-transfer system (Fig. 6a) not only avoids the complicated PVC-removing step, but also immobilizes Cl species into organic chlorides, which is a solution to the problem that the existing process is incompatible with PVC and realizes the utilization of waste Cl resource.

We further highlight the following limitations of the new system from a catalysis view deserving consideration and further development: a) improving the selectivity of a single Cl-containing product and preventing the undesirable side reactions (e.g. etherification, hydrodechlorination) by optimizing the catalyst's structure deserve increasing attention; b) Non-noble-metal based catalysts with comparable performance should be explored to improve the overall economic competitiveness; c) designing advanced active sites to convert the solid residue into higher-value liquid alkanes is highly desired; d) higher temperature generally favors the catalytic elimination of Cl species into HCl and therefore, great efforts should be devoted into improving the catalytic activity to reduce reaction temperature of the newly established system. Developments along these lines are going on in our labs.

Then, based on experimental data, we performed a preliminary mass balance analysis for the Cl-transfer process (Fig. 6b). Starting from 1000 kg waste PVC, 1010 kg of organic chlorides was obtained with the consumption of 664.6 kg THF only 13 kg $H_2$, meanwhile, 359.9 kg of Cl-free polymer was also formed, which can be easily converted with existing PE upcycling technologies. The key feature of the Cl-transfer is that the obtained organic chlorides have nearly the same high mass as that of waste PVC, showing that the newly established system adds a promising option with unequaled efficiency for the production of organic chlorides.

## 4. Conclusion

In summary, a Cl-transfer strategy converting waste PVC into organic

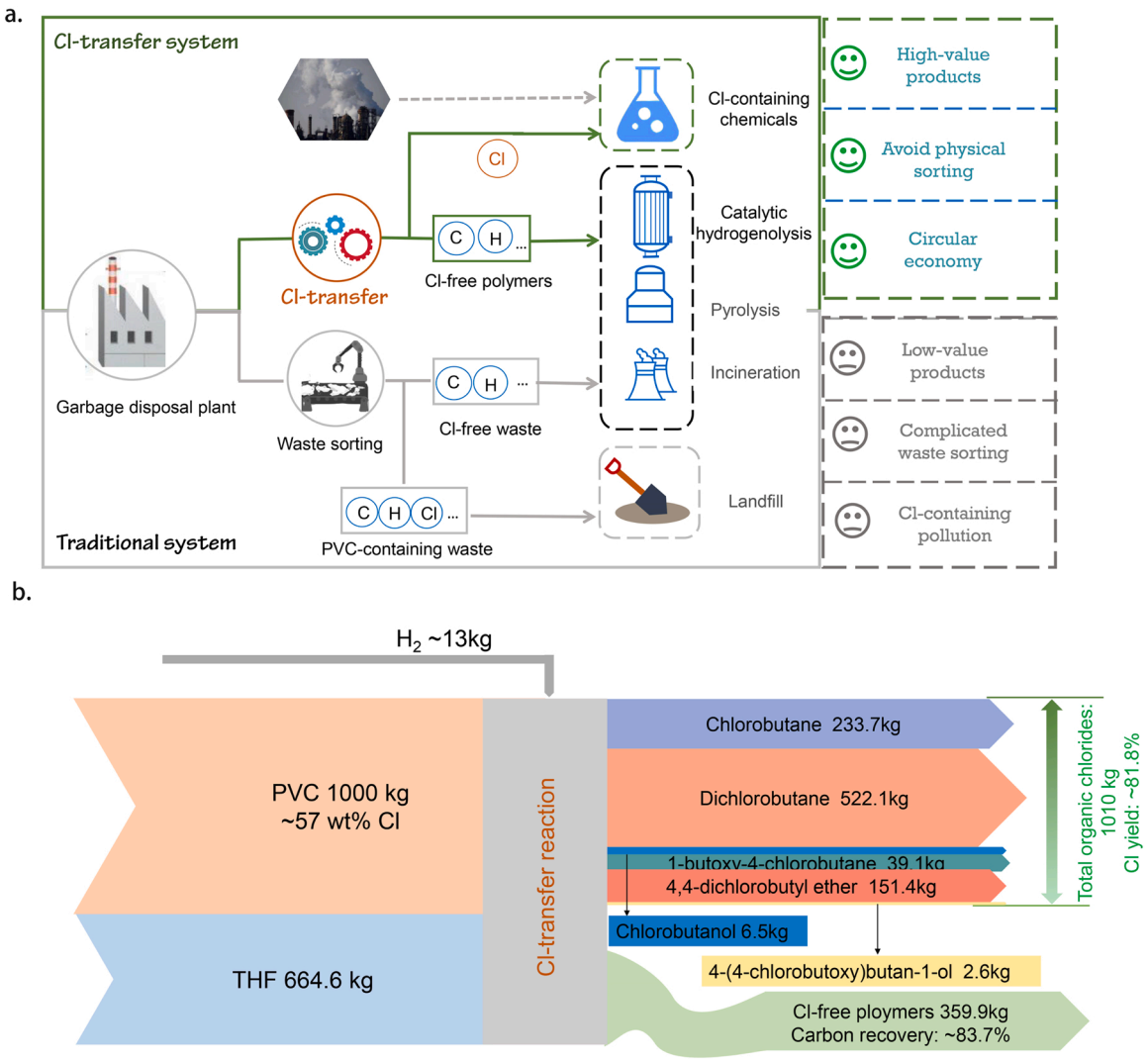


**Fig. 6.** (a) comparation of Cl-transfer and traditional systems; (b) the preliminary mass balance analysis for the Cl-transfer process.

chlorides and PE-like polymer with simple Cl acceptors over $Ru/Al_2O_3$ was developed to achieve PVC upcycling. The PE-like polymer can be converted by employing the upcycling methods of waste PE. This strategy allows the conversion of various real PVC waste and PVC-containing plastic mixtures and scale-up applications. The detailed Cl-transfer footprint was provided. The combination of Lewis acid and metal Ru sites could markedly promote the Cl-transfer reaction because of Lewis acid for the activation of C-O bonds and metal Ru sites for the activation of C-Cl bonds and the dissociation of $H_2$. By integrating Cl-transfer process into existing plastic treatment technologies, the new system shows great application potential and the preliminary mass balance displays the quality of feedstocks mainly flows to value-added organic chlorides. This work presents a novel Cl-transfer strategy to integrate PVC-containing plastic wastes into the production of chlorides and natural gas under the context of circular economy.

## CRediT authorship contribution statement

**Bo Feng:** Conceptualization, Methodology, Visualization, Formal analysis, Writing – original draft, Data curation. **Yaxuan Jing:** Conceptualization, Methodology, Visualization, Formal analysis, Writing – original draft, Data curation, Resources, Supervision, Funding acquisition, Project administration. **Yanqin Wang:** Conceptualization, Methodology, Visualization, Formal analysis, Writing – original draft, Data curation, Resources, Supervision, Funding acquisition, Project administration. **Xiaohui Liu:** Resources, Supervision. **Yong Guo:** Resources, Supervision. Overall direction of the project.

## Declaration of Competing Interest

The authors declare that they have no known competing financial interests or personal relationships that could have appeared to influence the work reported in this paper.

## Data Availability

The authors are unable or have chosen not to specify which data has been used.

## Acknowledgment

This work was supported financially by the NSFC of China (22102056, 21832002), China Postdoctoral Science Foundation (2021M691011 and 2021TQ0106), and Shanghai Super Postdoctoral Fellow.

## Appendix A. Supporting information

Supplementary data associated with this article can be found in the online version at doi:10.1016/j.apcatb.2023.122671.

## References


[1] R. Geyer, J.R. Jambeck, K.L. Law, Production, use, and fate of all plastics ever made, Sci. Adv. 3 (2017), https://doi.org/10.1126/sciadv.1700782 e1700782-e1700782.

[2] C. Jehanno, J.W. Alty, M. Roosen, S. De Meester, A.P. Dove, E.Y. Chen, F. A. Leibfarth, H. Sardon, Critical advances and future opportunities in upcycling commodity polymers, Nature 603 (2022) 803–814, https://doi.org/10.1038/s41586-021-04350-0.

[3] A.J. Martín, C. Mondelli, S.D. Jaydev, J. Pérez-Ramírez, Catalytic processing of plastic waste on the rise, Chem 7 (2021) 1487–1533, https://doi.org/10.1016/j.chempr.2020.12.006.

[4] S.R. Nicholson, N.A. Rorrer, A.C. Carpenter, G.T. Beckham, Manufacturing energy and greenhouse gas emissions associated with plastics consumption, Joule 5 (2021) 673–686, https://doi.org/10.1016/j.chempr.2020.12.006.

[5] M. Wey, J. Chen, H. Wu, W. Yu, T. Tsai, Formations and controls of HCl and PAHs by different additives during waste incineration, Fuel 85 (2006) 755–763, https://doi.org/10.1016/j.fuel.2005.09.011.

[6] M. Sadat-Shojai, G.-R. Bakhshandeh, Recycling of PVC wastes, Polym. Degrad. Stab. 96 (2011) 404–415, https://doi.org/10.1016/j.polymdegradstab.2010.12.001.

[7] B.R. Stanmore, The formation of dioxins in combustion systems, Combust. Flame 136 (2004) 398–427, https://doi.org/10.1016/j.combustflame.2003.11.004.

[8] J. Yu, L. Sun, C. Ma, Y. Qiao, H. Yao, Thermal degradation of PVC: a review, Waste Manag. 48 (2016) 300–314, https://doi.org/10.1016/j.wasman.2015.11.041.

[9] E.J.A.XvdS. Andŕe Wiersma, Marion A. den Hollander, Herman van Bekkum, Michiel Makkee, Jacob A. Moulijn, Comparison of the performance of activated carbon-supported noble metal catalysts in the hydrogenolysis of $CCl_2F_2$, J. Catal. 177 (1998) 29–39, https://doi.org/10.1006/jcat.1998.2091.

[10] H.S.Salvador Ordóñez, Fernando V. Díez, Hydrodechlorination of aliphatic organochlorinated compounds over commercial hydrogenation catalysts, Appl. Catal. B Environ. 25 (2000) 49–58, https://doi.org/10.1016/S0926-3373(99)00119-8.

[11] N. Barrabes, D. Cornado, K. Foettinger, A. Dafinov, J. Llorca, F. Medina, G. Rupprechter, Hydrodechlorination of trichloroethylene on noble metal promoted Cu-hydrotalcite-derived catalysts, J. Catal. 263 (2009) 239–246, https://doi.org/10.1016/j.jcat.2009.02.015.

[12] B.Z. Wu, H.Y. Chen, S.J. Wang, C.M. Wai, W. Liao, K. Chiu, Reductive dechlorination for remediation of polychlorinated biphenyls, Chemosphere 88 (2012) 757–768, https://doi.org/10.1016/j.chemosphere.2012.03.056.

[13] J. Poerschmann, B. Weiner, S. Woszidlo, R. Koehler, F.D. Kopinke, Hydrothermal carbonization of poly(vinyl chloride), Chemosphere 119 (2015) 682–689, https://doi.org/10.1016/j.chemosphere.2014.07.058.

[14] M.A. Keane, Catalytic conversion of waste plastics: focus on waste PVC, J. Chem. Technol. Biotechnol. 82 (2007) 787–795, https://doi.org/10.1002/jctb.1757.

[15] R. Lin, A.P. Amrute, J. Perez-Ramirez, Halogen-mediated conversion of hydrocarbons to commodities, Chem. Rev. 117 (2017) 4182–4247, https://doi.org/10.1021/acs.chemrev.6b00551.

[16] A.P.A. Ronghe Lin, Javier Pérez-Ramírez, Halogen-mediated conversion of hydrocarbons to commodities, Chem. Rev. 17 (2017) 4182–4247, https://doi.org/10.1021/acs.chemrev.6b00551.

[17] M.S.B. Kharasch, M. G, effect of organic peroxides in chlorination reactions, J. Org. Chem. 6 (1941) 810–817, https://doi.org/10.1021/jo01206a004.

[18] G.A.S. Olah, P. Renner, R. Kerekes, I, Radical reactions. I. Phosphorus chloride catalyzed chlorination of alkanes, cycloalkanes, and arylalkanes, J. Org. Chem. 39 (1974) 3472–3478, https://doi.org/10.1021/jo00938a003.

[19] D.E. Fagnani, D. Kim, S.I. Camarero, J.F. Alfaro, A.J. McNeil, Using waste poly (vinyl chloride) to synthesize chloroarenes by plasticizer-mediated electro(de) chlorination, Nat. Chem. 15 (2023) 222–229, https://doi.org/10.1038/s41557-022-01078-w.

[20] W.M. Qiao, S.H. Yoon, Y. Korai, I. Mochida, S. Inoue, T. Sakurai, T. Shimohara, Preparation of activated carbon fibers from polyvinyl chloride, Carbon 42 (2004) 1327–1331, https://doi.org/10.1016/j.carbon.2004.01.035.

[21] K.F. Toshiaki Yoshioka, Akitsugu Okuwaki, Chemical recycling of rigid-PVC by oxygen oxidation in NaOH solutions at elevated temperatures, Polym. Degrad. Stab. 67 (2000) 285–290, https://doi.org/10.1016/S0141-3910(99)00128-7.

[22] S. Ma, C. Cong, X. Meng, S. Cao, H. Yang, Y. Guo, X. Lu, S. Ma, Synthesis and on-target antibacterial activity of novel 3-elongated arylalkoxybenzamide derivatives as inhibitors of the bacterial cell division protein FtsZ, Bioorg. Med. Chem. Lett. 23 (2013) 4076–4079, https://doi.org/10.1016/j.bmcl.2013.05.056.

[23] A. Mizuno, N. Inomata, M. Miya, T. Kamei, M. Shibata, T. Tatsuoka, M. Yoshida, C. Takiguchi, T. Miyazaki, Synthesis and pharmacological evaluation of pyrroloazepine derivatives as potent antihypertensive agents with antiplatelet aggregation activity, Chem. Pharm. Bull. 47 (1999) 246–256, https://doi.org/10.1248/cpb.47.246.

[24] S. Tang, G.A. Baker, H. Zhao, Ether- and alcohol-functionalized task-specific ionic liquids: attractive properties and applications, Chem. Soc. Rev. 41 (2012) 4030–4066, https://doi.org/10.1002/chin.201232243.

[25] I. van der Veen, J. de Boer, Phosphorus flame retardants: properties, production, environmental occurrence, toxicity and analysis, Chemosphere 88 (2012) 1119–1153, https://doi.org/10.1016/j.chemosphere.2012.03.067.

[26] T. Yoshioka, T. Kameda, S. Imai, A. Okuwaki, Dechlorination of poly(vinyl chloride) using NaOH in ethylene glycol under atmospheric pressure, Polym. Degrad. Stab. 93 (2008) 1138–1141, https://doi.org/10.1016/j.polymdegradstab.2008.03.007.

[27] J.B. Pedley, R.D. Naylor, S.P. Kirby, Standard enthalpies of formation derived from experimental data, in: Thermochemical Data of Organic Compounds, Springer, Dordrecht, 1986, https://doi.org/10.1007/978-94-009-4099-4_2.

[28] T.Tb Tetsuya Yoneda, Kenji Konuma, Hydrodechlorination of para-substituted chlorobenzenes over a ruthenium/ carbon catalyst, Appl. Catal. B Environ. 84 (2008) 667–677, https://doi.org/10.1016/j.apcatb.2008.05.024.

[29] M. Martin-Martinez, A. Álvarez-Montero, L.M. Gómez-Sainero, R.T. Baker, J. Palomar, S. Omar, S. Eser, J.J. Rodriguez, Deactivation behavior of Pd/C and Pt/C catalysts in the gas-phase hydrodechlorination of chloromethanes: structure–reactivity relationship, Appl. Catal. B Environ. 162 (2015) 532–543, https://doi.org/10.1016/j.apcatb.2014.07.017.

[30] M. Martin-Martinez, L.M. Gomez-Sainero, M.A. Alvarez-Montero, J. Bedia, J. J. Rodriguez, Comparison of different precious metals in activated carbon-supported catalysts for the gas-phase hydrodechlorination of chloromethanes, Appl. Catal. B Environ. 132 (2013) 256–265, https://doi.org/10.1016/j.apcatb.2012.11.041.

[31] L.M. Gomez-Sainero, X.L. Seoane, J.L.G. Fierro, A. Arcoya, Liquid-phase hydrodechlorination of $CCl_4$ to $CHCl_3$ on Pd/carbon catalysts: Nature and role of Pd active species, J. Catal. 209 (2002) 279–288, https://doi.org/10.1006/jcat.2002.3655.

[32] P.P. Kulkarni, S.S. Deshmukh, V.I. Kovalchuk, J.L. d'Itri, Hydrodechlorination of dichlorodifluoromethane on carbon-supported Group VIII noble metal catalysts, Catal. Lett. 61 (1999) 161–166, https://doi.org/10.1023/A:1019005813080.

[33] H. Liu, J. Yang, Y. Jia, Z. Wang, M. Jiang, K. Shen, H. Zhao, Y. Guo, Y. Guo, L. Wang, S. Dai, W. Zhan, Significant improvement of catalytic performance for chlorinated volatile organic compound oxidation over RuOx supported on acid-etched $Co_3O_4$, Environ. Sci. Technol. 55 (2021) 10734–10743, https://doi.org/10.1021/acs.est.1c02970.

[34] S.K. Kaiser, R. Lin, F. Krumeich, O.V. Safonova, J. Perez-Ramirez, Preserved in a shell: high-performance graphene-confined ruthenium nanoparticles in acetylene hydrochlorination, Angew. Chem. Int. Ed. 58 (2019) 12297–12304, https://doi.org/10.1002/anie.201906916.

[35] C. Mondelli, G. Gozaydin, N. Yan, J. Perez-Ramirez, Biomass valorisation over metal-based solid catalysts from nanoparticles to single atoms, Chem. Soc. Rev. 49 (2020) 3764–3782, https://doi.org/10.1039/d0cs00130a.

[36] Y.-H.L. Manhao Zeng, Garrett Strong, Anne M. LaPointe, Andrew L. Kocen, Zhiqiang Qu, Geoffrey W. Coates, Susannah L. Scott, Mahdi M. Abu-Omar, Chemical upcycling of polyethylene to value-added α,ω-divinylfunctionalized oligomers, ACS Sustain. Chem. Eng. 9 (2021) 13926–13936, https://doi.org/10.1021/acssuschemeng.1c05272.s001.

[37] C.M. Plummer, H. Zhou, W. Zhu, H. Huang, L. Liu, Y. Chen, Mild halogenation of polyolefins using an N-haloamide reagent, Polym. Chem. 9 (2018) 1309–1317, https://doi.org/10.1039/c8py00013a.

[38] M. Tamura, S. Miyaoka, Y. Nakaji, M. Tanji, S. Kumagai, Y. Nakagawa, T. Yoshioka, K. Tomishige, Structure-activity relationship in hydrogenolysis of polyolefins over Ru/support catalysts, Appl. Catal. B Environ. 318 (2022) 121780–121794, https://doi.org/10.1016/j.apcatb.2022.121870.

[39] Y. Nakaji, M. Tamura, S. Miyaoka, S. Kumagai, M. Tanji, Y. Nakagawa, T. Yoshioka, K. Tomishige, Low-temperature catalytic upgrading of waste polyolefinic plastics into liquid fuels and waxes, Appl. Catal. B Environ. 285 (2021), https://doi.org/10.1016/j.apcatb.2020.119805, 119805-119014.

[40] F.D.B. Wei-Tse Lee, Antoine P. van Muyden, Kun-Han Lin, Clémence Corminboeuf, Reza R. Zamani, Paul J. Dyson, Catalytic hydrocracking of synthetic polymers into grid-compatible gas streams, Cell Rep. Phys. Sci. 2 (2021), 100332, https://doi.org/10.2139/ssrn.3696768.

[41] J.E. Rorrer, C. Troyano-Valls, G.T. Beckham, Y. Román-Leshkov, Hydrogenolysis of polypropylene and mixed polyolefin plastic waste over Ru/C to produce liquid alkanes, ACS Sustain. Chem. Eng. 9 (2021) 11661–11666, https://doi.org/10.1021/acssuschemeng.1c03786.s001.

[42] P.A. Kots, B.C. Vance, D.G. Vlachos, Polyolefin plastic waste hydroconversion to fuels, lubricants, and waxes: a comparative study, React. Chem. Eng. 7 (2022) 41–54, https://doi.org/10.1039/d1re00447f.

[43] L. Chen, Y. Zhu, L.C. Meyer, L.V. Hale, T.T. Le, A. Karkamkar, J.A. Lercher, O. Y. Gutiérrez, J. Szanyi, Effect of reaction conditions on the hydrogenolysis of polypropylene and polyethylene into gas and liquid alkanes, React. Chem. Eng. 7 (2022) 844–854, https://doi.org/10.1039/d1re00431j.

[44] R.S. Suppino, R. Landers, A.J.G. Cobo, Influence of noble metals (Pd, Pt) on the performance of Ru/Al2O3 based catalysts for toluene hydrogenation in liquid phase, Appl. Catal. A-Gen. 525 (2016) 41–49, https://doi.org/10.1016/j.apcata.2016.06.038.

[45] M.A. Vicerich, V.M. Benitez, M.A. Sánchez, C. Especel, F. Epron, C.L. Pieck, Ru-Pt catalysts supported on $Al_2O_3$ and $SiO_2$—$Al_2O_3$ for the selective ring opening of naphthenes, Can. J. Chem. Eng. 98 (2019) 749–756, https://doi.org/10.1002/cjce.23656.

[46] V.B. Saptal, T. Sasaki, B.M. Bhanage, Ru@PsIL catalysed synthesis of n-formamides and benzimidazole using carbon dioxide and dimethylamine borane, ChemCatChem 10 (2018) 2593–2600, https://doi.org/10.1002/cctc.201800185.

[47] S.E. Clapham, A. Hadzovic, R.H. Morris, Mechanisms of the H2-hydrogenation and transfer hydrogenation of polar bonds catalyzed by ruthenium hydride complexes,

Coord. Chem. Rev. 248 (2004) 2201–2237, https://doi.org/10.1016/j.ccr.2004.04.007.
[48] C. Coperet, D.P. Estes, K. Larmier, K. Searles, Isolated surface hydrides: formation, structure, and reactivity, Chem. Rev. 116 (2016) 8463–8505, https://doi.org/10.1021/acs.chemrev.6b00082.
[49] W.T. Bolleter, The infrared spectra of some chlorinated hydrocarbons in the cesium bromide region, Appl. Spectrosc. 18 (3) (1964) 72–78, https://doi.org/10.1366/000370264789620600.
[50] J.J. Mannion, T.S. Wang, Infrared absorption characteristic of -C≡C-$CH_2$- linkage, Spectrochim. Acta 17 (1961) 990–1000, https://doi.org/10.1016/0371-1951(61)80034-9.
[51] D. Baudouin, K.C. Szeto, P. Laurent, A. De Mallmann, B. Fenet, L. Veyre, U. Rodemerck, C. Coperet, C. Thieuleux, Nickel-silicide colloid prepared under mild conditions as a versatile Ni precursor for more efficient $CO_2$ reforming of $CH_4$ catalysts, J. Am. Chem. Soc. 134 (2012) 20624–20627, https://doi.org/10.1021/ja3111797.
[52] E. Wiercigroch, E. Szafraniec, K. Czamara, M.Z. Pacia, K. Majzner, K. Kochan, A. Kaczor, M. Baranska, K. Malek, Raman and infrared spectroscopy of carbohydrates: a review, Spectrochim. Acta A Mol. Biomol. 185 (2017) 317–335, https://doi.org/10.1016/j.saa.2017.05.045.
[53] H.Z. Lihui Lu, Tianfu Wang, Jianeng Wu, Fangming Jin, Toshiaki Yoshioka, new strategy for $CO_2$ utilization with waste plastics- conversion of hydrogen carbonate into formate using polyvinyl chloride in water, Green Chem. 22 (2020) 352, https://doi.org/10.1039/c9gc02484k.
[54] Yu Xin, Y. Jing, Lin Dong, Xiaohui Liu, Yong Guo, Yanqin Wang, Selective production of indane and its derivatives from lignin over a modified niobium-based catalyst, Chem. Commun. 55 (2019) 9391–9394, https://doi.org/10.1039/c9cc04101j.
[55] Q.W. Dan Wu, Olga V. Safonova, Deizi V. Peron, Wenjuan Zhou, Zhen Yan, Maya Marinova, Andrei Y. Khodakov, Vitaly V. Ordomsky, Lignin compounds to monoaromatics: selective cleavage of C-O bonds over a brominated ruthenium catalyst, Angew. Chem. Int. Ed. 60 (2021) 12513–12523, https://doi.org/10.1002/ange.202101325.
[56] V.P.K. Chakravartula, S. Srikanth, Balaga Viswanadham, Komandur V.R. Chary, Hydrodechlorination of 1,2,4-trichlorbenzene over supported ruthenium catalysts on various supports, Catal. Commun. 13 (2011) 69–72, https://doi.org/10.1016/j.catcom.2011.06.011.
[57] S. Omar, J. Palomar, L.M. Gómez-Sainero, M.A. Álvarez-Montero, M. Martin-Martinez, J.J. Rodriguez, Density functional theory analysis of dichloromethane and hydrogen interaction with Pd clusters: first step to simulate catalytic hydrodechlorination, J. Phys. Chem. C 115 (2011) 14180–14192, https://doi.org/10.1021/jp200329j.
[58] M. Tian, Z. Jiang, C. Chen, M. Kosari, X. Li, Y. Jian, Y. Huang, J. Zhang, L. Li, J.-W. Shi, Y. Zhao, C. He, Engineering Ru/$MnCo_3O_x$ for 1,2-dichloroethane benign destruction by strengthening C–Cl cleavage and chlorine desorption: decisive role of $H_2O$ and reaction mechanism, ACS Catal. (2022) 8776–8792, https://doi.org/10.1021/acscatal.2c02304.
[59] A.M.M. Bonarowska, Z. Karpińnski, Hydrogenolysis of C–C and C–Cl bonds by Pd–Re $Al_2O_3$ catalysts, Appl. Catal. A-Gen. 188 (1999) 145–154, https://doi.org/10.1016/S0926-860X(99)00241-0.
[60] V. Coessens, T. Pintauer, K. Matyjaszewski, Functional polymers by atom transfer radical polymerization, Prog. Polym. Sci. 26 (2001) 337–377, https://doi.org/10.1016/S0079-6700(01)00003-X.